REPORT DOCUMENTATION PAGE

2

Form Approved OMB NO. 0704-0188

1. REPORT DATE (DD-MM-YYYY)	2. REPORT TYPE	3. DATES COVERED (From - To)
	New Reprint	-

4. TITLE AND SUBTITLE	5a. CONTRACT NUMBER
Extraordinary Photocurrent Harvesting at Type-II HeterojunctionInterfaces: Toward High Detectivity Carbon Nanotube InfraredDetectors	W911NF-09-1-0295
	5b. GRANT NUMBER
	5c. PROGRAM ELEMENT NUMBER
	611102

6. AUTHORS	5d. PROJECT NUMBER
Rongtao Lu, Caleb Christianson, Alec Kirkeminde , Shenqiang Ren, Judy Wu	
	5e. TASK NUMBER
	5f. WORK UNIT NUMBER

7. PERFORMING ORGANIZATION NAMES AND ADDRESSES	8. PERFORMING ORGANIZATION REPORT NUMBER
University of Kansas Center for Research, Inc. University of Kansas Center for Research, Inc. 2385 Irving Hill Road Lawrence, KS 66045 -7568	

9. SPONSORING/MONITORING AGENCY NAME(S) AND ADDRESS(ES)	10. SPONSOR/MONITOR'S ACRONYM(S)
U.S. Army Research Office P.O. Box 12211 Research Triangle Park, NC 27709-2211	ARO
	11. SPONSOR/MONITOR'S REPORT NUMBER(S)
	56050-EL.19

12. DISTRIBUTION AVAILIBILITY STATEMENT
Approved for public release; distribution is unlimited.

13. SUPPLEMENTARY NOTES
The views, opinions and/or findings contained in this report are those of the author(s) and should not contrued as an official Department of the Army position, policy or decision, unless so designated by other documentation.

14. ABSTRACT

Despite the potentials and the efforts put in the
development of uncooled carbon nanotube infrared detectors
during the past two decades, their figure-of-merit detectivity
remains orders of magnitude lower than that of conventional
semiconductor counterparts due to the lack of efficient exciton

15. SUBJECT TERMS
carbon nanotube, infrared detector, heterojunction

16. SECURITY CLASSIFICATION OF:			17. LIMITATION OF ABSTRACT	15. NUMBER OF PAGES	19a. NAME OF RESPONSIBLE PERSON
a. REPORT	b. ABSTRACT	c. THIS PAGE			Judy Wu
UU	UU	UU	UU		19b. TELEPHONE NUMBER
					785-864-3240

Report Title

Extraordinary Photocurrent Harvesting at Type-II HeterojunctionInterfaces: Toward High Detectivity Carbon Nanotube InfraredDetectors

ABSTRACT

Despite the potentials and the efforts put in the
development of uncooled carbon nanotube infrared detectors
during the past two decades, their figure-of-merit detectivity
remains orders of magnitude lower than that of conventional
semiconductor counterparts due to the lack of efficient exciton
dissociation schemes. In this paper, we report an extraordinary
photocurrent harvesting configuration at a semiconducting
single-walled carbon nanotube (s-SWCNT)/polymer type-II
heterojunction interface, which provides highly efficient
exciton dissociation through the intrinsic energy offset by designing the s-SWCNT/polymer interface band alignment. This
results in significantly enhanced near-infrared detectivity of 2.3×108 cm·Hz1/2/W, comparable to that of the many conventional
uncooled infrared detectors. With further optimization, the s-SWCNT/polymer nanohybrid uncooled infrared detectors could be
highly competitive for practical applications.

REPORT DOCUMENTATION PAGE (SF298)
(Continuation Sheet)

Continuation for Block 13

ARO Report Number   56050.19-EL
Extraordinary Photocurrent Harvesting at Type-I   ...

Block 13: Supplementary Note
© 2012 . Published in Nano Letters, Vol. Ed. 0 12, (11) (2012), ((11). DoD Components reserve a royalty-free, nonexclusive
and irrevocable right to reproduce, publish, or otherwise use the work for Federal purposes, and to authroize others to do so
(DODGARS §32.36). The views, opinions and/or findings contained in this report are those of the author(s) and should not be
construed as an official Department of the Army position, policy or decision, unless so designated by other documentation.

Approved for public release; distribution is unlimited.

NANO LETTERS

Extraordinary Photocurrent Harvesting at Type-II Heterojunction Interfaces: Toward High Detectivity Carbon Nanotube Infrared Detectors

Rongtao Lu,*,[†] Caleb Christianson,[†] Alec Kirkeminde,[‡] Shenqiang Ren,[‡] and Judy Wu*,[†]

[†]Department of Physics and Astronomy, University of Kansas, Lawrence, Kansas 66045, United States
[‡]Department of Chemistry, University of Kansas, Lawrence, Kansas 66045, United States

S Supporting Information

ABSTRACT: Despite the potentials and the efforts put in the development of uncooled carbon nanotube infrared detectors during the past two decades, their figure-of-merit detectivity remains orders of magnitude lower than that of conventional semiconductor counterparts due to the lack of efficient exciton dissociation schemes. In this paper, we report an extraordinary photocurrent harvesting configuration at a semiconducting single-walled carbon nanotube (s-SWCNT)/polymer type-II heterojunction interface, which provides highly efficient

exciton dissociation through the intrinsic energy offset by designing the s-SWCNT/polymer interface band alignment. This results in significantly enhanced near-infrared detectivity of 2.3×10^8 cm·Hz$^{1/2}$/W, comparable to that of the many conventional uncooled infrared detectors. With further optimization, the s-SWCNT/polymer nanohybrid uncooled infrared detectors could be highly competitive for practical applications.

KEYWORDS: Infrared detector, carbon nanotube, P3HT, type-II heterojunction, detectivity
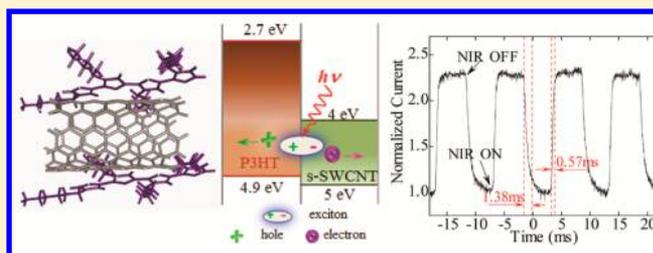
Single-wall carbon nanotubes (SWCNTs) have outstanding photoabsorption in the infrared (IR) spectrum, making them promising candidates for IR detector applications.[1−8] However, the photon-generated excitons in SWCNTs remain strongly bonded due to the enhanced Coulomb interaction and the reduced screen effect in one-dimensional materials,[4,9] resulting in difficulties in exciton dissociation and hence photocurrent generation in SWCNTs. Consequently, SWCNTs based IR detectors are mostly thermal type, or bolometers, since the excitons dissociate primarily through thermal interactions with the carbon nanotube lattice,[10,11] and the reported low figure-of-merit detectivity $D^* \sim 10^5–10^6$ cm·Hz$^{1/2}$/W[6,8,12] is several orders of magnitude lower than that of conventional uncooled IR detectors.[13] An additional drawback of these SWCNT bolometers is the slow photo-response on the order of tens of milliseconds or longer, indicative of the strong influence of the slow surface oxygen desorption/adsorption.[3] The implementation of efficient exciton dissociation schemes represents a critical step toward high-performance SWCNT IR detectors.

Type-II heterojunctions formed at the interface between semiconducting SWCNTs (s-SWCNTs) and another selected semiconductor may provide a promising scheme for exciton dissociation by designing band edge alignment at the interface. The resulted energy offset, which exceeds the exciton binding energy, will facilitate the dissociation of excitons on a much faster time scale than recombination after they are generated upon IR photon absorption in s-SWCNTs.[14] In particular, the

type-II heterojunctions formed at the interface of s-SWCNT and semiconducting polymer have unique advantages in terms of nonvacuum based processing and low cost. Poly(3-hexylthiophene) (P3HT) is among several semiconducting conjugated polymers that have appropriate band offsets to s-SWCNTs, and the type-II heterojunction interface formed with electron accepting s-SWCNTs is shown schematically in Figure 1a and b.[14,15] The s-SWCNT/P3HT constitutes a donor–acceptor system, where an s-SWCNT works as an electron acceptor due to its higher electron affinity.[14] Considering that the diameters of the s-SWCNTs used in this experiment are in the range of 1.2−1.7 nm, the exciton binding energy is estimated to be below 0.5 eV.[16] Therefore, the 1.3 eV offset between the conduction band of s-SWCNT and the lowest unoccupied molecular orbital of P3HT is considerably greater than the exciton binding energy of less than 0.5 eV in the s-SWCNTs used in our experiments.[16] This means that the photogenerated excitons could be efficiently dissociated at the s-SWCNT/P3HT interface, which is followed by free electron transfer to s-SWCNTs and hole injection into P3HT, resulting in enhanced photoconductivity upon incident near IR (NIR) illumination. This exciton dissociation mechanism is consistent with the observation of a greatly enhanced charge-separated state and dramatically lengthened free carrier decay with
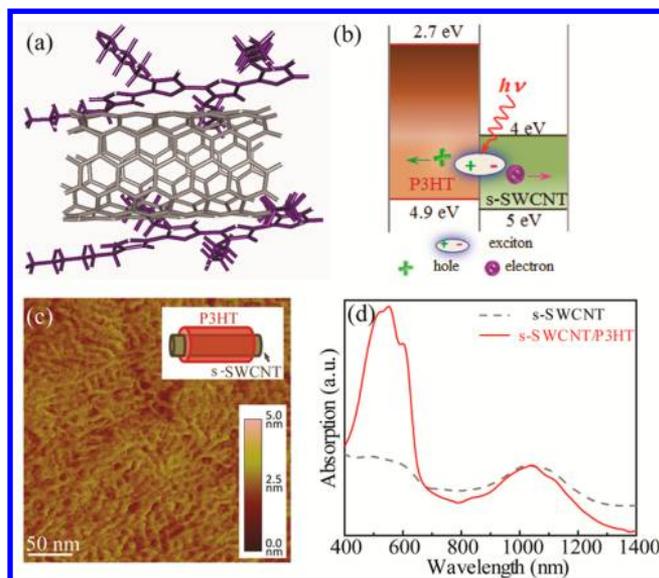
Figure 1. (a) Diagram of s-SWCNT/P3HT nanohybrid. (b) Band structure of the s-SWCNT/P3HT type-II heterojunction. (c) AFM image of s-SWCNT/P3HT. (d) Optical absorbance spectra of s-SWCNT and s-SWCNT/P3HT.

increasing s-SWCNT concentration in the s-SWCNT/P3HT composite.[15] In the s-SWCNT/P3HT nanohybrid NIR detector, NIR photons are absorbed by the SWCNTs. The NIR photogenerated excitons on SWCNTs, which may have higher binding energy compared to their counterparts in the s-SWCNT/P3HT solar cells due to the one-dimensional nature of the SWCNT, are expected to dissociate via the same mechanism as described above in the solar cell case. Indeed, in this experiment a significantly enhanced photocurrent was observed in the s-SWCNT/P3HT nanohybrids NIR detectors, which results in a greatly improved D^*, up to 2.3×10^8 cm·Hz/$W^{1/2}$, and fast photoresponse with a response time on the order of 1 ms, making SWCNT-based NIR detectors competitive, for the first time, to their conventional counterparts.

It is important, however, to differentiate this work from previous reports on SWCNT/polymer composite NIR detectors.[17−21] First, the desired type-II heterojunction only forms on the s-SWCNTs. The band offset on the interface between metallic SWCNTs (m-SWCNTs) and P3HT is unfavorable,[22] and the presence of the m-SWCNTs is in fact detrimental since excitons get quenched by transferring electrons from filled states at the m-SWNT Fermi level to the P3HT highest occupied molecular orbital.[15] It is therefore critical to use sorted s-SWCNTs instead of the as-made SWCNTs, which typically contain a 1/3 volume portion of m-SWCNTs and have been used for most of the previously reported SWCNT/polymer composite IR detectors. On the other hand, the selection of the polymer semiconductors is critical, and out of many that were tested, only a few were confirmed to form the desired type-II heterojunctions with s-SWCNTs.[14] Finally, the s-SWCNTs must be well-dispersed in the polymer to avoid bundling, which has been found critical to achieving a well-defined type-II interface that is necessary for efficient exciton dissociation.[23,24] It is reported that the interaction between s-SWCNT and P3HT via π−π stacks overcome the van der Waals interaction between s-SWCNTs and provide efficient interfacial area for charge separation, which is only possible if the s-SWCNTs are individually

embedded in an P3HT matrix.[24] This argument is supported by the dramatically improved photocurrent which was only demonstrated on the s-SWCNT/P3HT nanohybrid solar cells using a specially developed solution self-assembly approach to ensure the s-SWCNT dispersion.[23] Based on these arguments, it is not surprising that most SWCNT/polymer composite IR detectors reported previously are primarily based on either completely or predominantly thermal effects as evidenced in the disappointingly low D^* and slow photoresponse.[17−21] In contrast, this work reports an extraordinary photocurrent harvesting scheme of forming type-II heterojunction at the interface between well-dispersed s-SWCNTs and conjugated P3HT polymer for high efficiency exciton dissociation. With further optimizations, the scheme may provide a low-cost pathway toward high-performance s-SWCNT IR detectors competitive to conventional uncooled IR detectors.

A self-assembly solution approach was applied to facilitate P3HT helical conformations onto the s-SWCNT core prior to the s-SWCNT/P3HT deposition. This is crucial to the formation of the π-conjugation of the polymer at the interface with the s-SWCNT to enable formation of the type-II heterojunctions. It has been shown that P3HT adsorbs rapidly, beginning in solution, to the s-SWCNT through π−π stacking forces.[23] The assembly of a larger set of chains and s-SWNT is what occurs during a typical s-SWCNT/P3HT film preparation, and a diagram of the s-SWCNT/P3HT nanohybrid is shown in Figure 1a.

High-purity (∼98%) s-SWCNTs with nominal diameter in the range 1.2−1.7 nm and length in the range 300 nm to 5 μm (IsoNanotube-S from NanoIntegris) were used in this study. The use of s-SWCNTs with larger diameter would be advantageous due to their lower exciton binding energy that scales as ∼$1/d$[16] and larger carrier mobility in the diffusive transport regime that scales as d^2.[25] The s-SWCNT/P3HT (core/shell) nanohybrids were prepared in 10 mg/mL 1,2-dichlorobenzene (1,2-DCB) solution containing P3HT and s-SWCNT (3 wt %).[23] Nonsolvent acetonitrile was adopted to promote P3HT aggregation onto SWCNT surface. A sonication step was implemented to assist self-assembly of P3HT polymer backbone onto s-SWCNTs. The s-SWCNT/P3HT nanohybrid films were prepared by spin-coating the solution at 1000 rpm for 1 min on a silicon substrate with a 500 nm thick thermal oxide layer on top. The s-SWCNT/P3HT nanohybrid film thickness is around 35−70 nm. Smaller thicknesses were found to be advantageous to harvesting larger photocurrents considering the small charge carrier diffusion length of a few nanometers in polymers such as P3HT.[26] Ti(10 nm)/Au(50 nm) electrodes were predeposited on the substrates using electron beam evaporation. Control samples of pure s-SWCNT and pure P3HT films were fabricated and characterized (see Supporting Information).

The atomic force microscopy (AFM) image of Figure 1c shows wormlike morphology in the s-SWCNT/P3HT films typically of few μm long. The AFM image indicates that a percolation network consisting of a large number of individual s-SWCNT/P3HT units was formed in the film. This is consistent with the previous report on the s-SWCNT/P3HT nanohybrid processed using a similar condition,[23] suggesting that the core−shell structure is well-formed. The diameter of individual s-SWCNT/P3HT is about several nanometers based on the transmission electron microscopy study (see Supporting Information, Figure S1). In the photoactive layer, the s-SWCNTs work as electron acceptors due to their higher
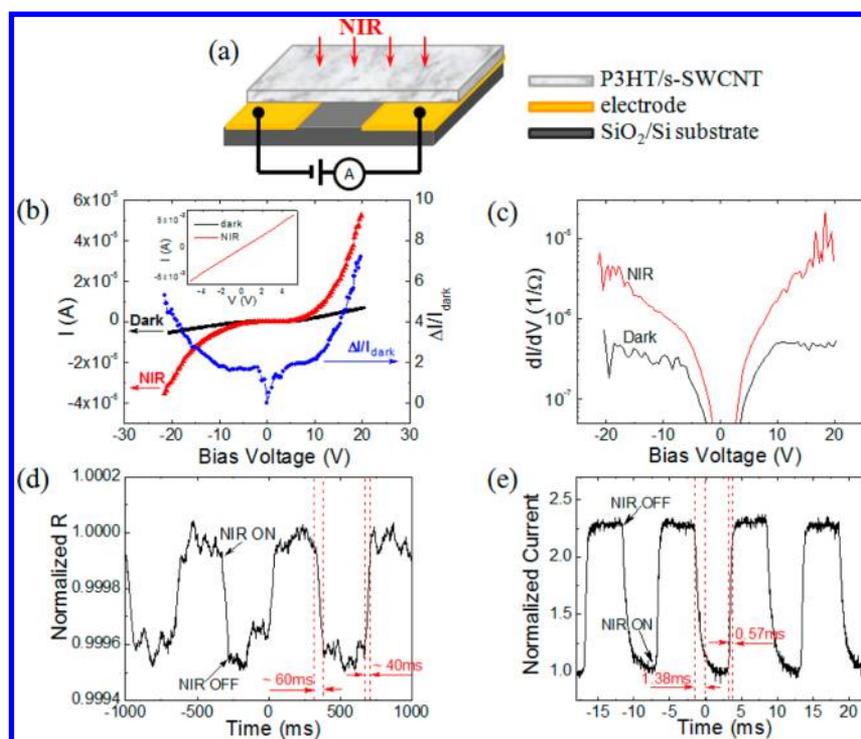
Figure 2. (a) Brief diagram of the electrical setup for IR detections. (b) Representative V−I curves of s-SWCNT/P3HT in dark and under NIR illumination of 2 mW/mm^2. The inset shows the voltage biased V−I curves of s-SWCNT control sample. (c) Differential conductance dI/dV of s-SWCNT/P3HT: the data were calculated from b. (d) Current biased temporal response of pure s-SWCNT under 1.5 Hz NIR modulation with intensity of 0.3 mW/mm^2, bias current 50 mA. (e) s-SWCNT/P3HT nanohybrid under 99 Hz NIR modulation with an intensity of 0.35 mW/mm^2 and bias voltage was 10 V. The response time was calculated using 10−90% magnitude change. All measurements were taken at room temperature.

electron affinity compared to the P3HT. Figure 1b shows the band alignment in the active layer.

A Cary 5000 ultraviolet−visible−NIR dual-beam spectrophotometer was used for the optical absorbance spectra measurement of the s-SWCNT and s-SWCNT/P3HT dispersed in 1,2-DCB. Representative absorption spectra of the s-SWCNT and s-SWCNT/P3HT nanohybrid are depicted in Figure 1d. For transport characterization, the setup shown in Figure 2a was employed. The voltage bias for voltage (V)−current (I) curve measurement was applied using an Agilent E3631A voltage source, and current was examined by measuring the voltage through a constant resistor in series, typically 10−100 kΩ, using a HP 34420A voltmeter. Temporal response was measured using an Agilent 54624A oscilloscope. The noise spectrum was measured using a Keithley 224 current source and a Stanford Research SR760 spectrum analyzer and then converted into current noise spectrum using the corresponding dynamic resistance. NIR light was produced from a xenon light source with NIR filter (1.0−1.3 μm bandpass). The power intensity was calibrated by using a Thorlabs PM100D power meter, and IR modulation was controlled using a mechanical chopper. The IR power incident on the detection element is calculated from the calibrated power intensity and detection element area, which is defined by the sample width of 4 mm and electrode spacing of 0.35−0.7 mm. S-SWCNT/P3HT samples were mounted in an optical cryostat during the measurements.

Based on the Kataura plot[27] and the nominal SWCNTs diameter range, optical absorption from the s-SWCNTs in our samples is predicted to occur in two bands at approximately 800−1200 nm (S_{22} transitions) and 1400−2000 nm (S_{11} transitions). The optical absorption spectra of the s-SWCNTs and s-SWCNT/P3HT core/shell nanohybrids in 1,2-DCB

match this prediction well, as shown in Figure 1d. In addition, a strong absorption peak at 610 nm was also observed on the s-SWCNT/P3HT core/shell nanohybrids, indicative of a highly structured order in the P3HT polymer layer after coating onto the s-SWCNT cores.[28] The P3HT conjugated polymer is photoactive in the visible range (<630 nm wavelength) rather than the IR range. Therefore, the absorption and photocurrent excited by the NIR light are anticipated only from the s-SWCNTs in the s-SWCNT/P3HT nanohybrid.

Strong NIR photoresponses in s-SWCNT/P3HT were observed in electrical transport characterizations. The V−I curves of a representative s-SWCNT/P3HT nanohybrid sample in dark and NIR illumination of ∼2 mW/mm^2 are shown in Figure 2b. The V−I curves are highly nonlinear. The V−I in dark (black curve) behaves like two Schottky diodes connected inversely. When the s-SWCNT/P3HT nanohybrid is illuminated by the NIR light (red curve), the current increases dramatically, and the V−I curve turns much more nonlinear with a very clear bend-up at a voltage around ±5 V. This can be clearly identified from the calculated current response ΔI over dark current I_{dark} ratio (blue curve), as shown in Figure 2b. The $\Delta I/I_{dark}$ ratio increases monotonically with the bias voltage and reaches a ratio of 7 at 20 V bias. This large photocurrent suggests that highly efficient exciton dissociation can be provided by the type-II heterojunctions formed at the s-SWCNT/P3HT interface. On the contrary, the voltage biased V−I curves of the s-SWCNT control sample in dark and under NIR illumination overlap with each other, as shown in the inset of Figure 2b, indicative of negligible photoresponse in absence of the exciton dissociation mechanism. To quantify the photoconductance, Figure 2c shows the differential photoconductance dI/dV for an s-SWCNT/P3HT nanohybrid

sample under NIR illumination, which is about 10−20 times of the dark conductance. This is in contrast to the nearly unchanged dI/dV observed on the s-SWCNT control sample with and without NIR illumination (see Supporting Information, Figure S3). The much higher photoconductance in the s-SWCNT/P3HT nanhybrid device as opposed to the negligible one in the s-SWCNT control sample may be attributed to the efficient exciton dissociation mechanism at the s-SWCNT/P3HT interface. Upon exciton dissociation, the holes (electrons) are injected into P3HT (s-SWCNT), resulting in improved conductivity by more than an order of magnitude as shown in Figure 2c. This large photoconductivity enhancement is consistent with the high internal quantum efficiency (IQE) up to 86% in the s-SWCNT/P3HT nanohybrid under the experimental conditions of this work (see Supporting Information) and supports the argument of high-efficiency exciton dissociation facilitated by the type II heterojunction at the s-SWCNT/P3HT interface.

The role of the type-II heterojunctions formed at the s-SWCNT/P3HT interface in exciton dissociation is further demonstrated by comparing the differences in the temporal photoresponse curves of the s-SWCNT film and s-SWCNT/P3HT nanohybrid samples, as shown in Figure 2c and 2d, respectively. In the former, low resistance (R) change of about 0.06% under 0.3 mW/mm^2 NIR illumination was observed, plus a larger response time of 40−60 ms, which is calculated from 10% to 90% magnitude change corresponding to "NIR ON" or "NIR OFF". Because of the slow photoresponse, the IR modulation frequency was limited to only a few hertz in the measurements of the s-SWCNT samples. It should be noted that this response time is actually comparable with that obtained on suspended as-made SWCNT films,[5,6] which is much smaller than that reported in unsuspended as-made SWCNTs due to enhanced thermal response at reduced thermal link between the CNT detector and the environment by suspending the SWCNT film.[3,6] Compared with the unsuspended as-made SWCNT films, the improved thermal response in s-SWCNT films may be attributed to the elimination of m-SWCNT "shorts" in the percolation path. Nevertheless, the photoresponse in s-SWCNT is very small and comparable to that of the as-made SWCNT films in the suspended form.[6] This is not surprising considering the lack of exciton dissociation mechanism in SWCNTs and the elimination of m-SWCNTs will not change the thermal nature of the photoresponse in the s-SWCNT films. On the contrary, a much larger and faster temporal response was observed on the s-SWCNT/P3HT nanohybrid samples as shown in Figure 2d. At 10 V bias and 0.35 mW/mm^2, the observed photocurrent is more than twice of the dark current, corresponding to a photoresponse that is more than 2 orders of magnitude higher than that of the s-SWCNT samples. In addition, the response times of 0.6 ms (NIR ON) and 1.4 ms (NIR OFF), respectively, are more than an order of magnitude smaller than that of the s-SWCNT. Interestingly, the response profile is not symmetric, and the "OFF" response takes slightly longer as seen by the presence of a small tail. Since a similar asymmetric temporal profile was reported also on other SWCNT/polymer composites with much longer tails after the IR is off, the small tail at the very end of the NIR OFF curve may be attributed to the minor thermal effect in the nanohybrid. Nevertheless, the previously reported IR response time of about 60 ms on SWCNT/polymer composites[17,18] is significantly longer than that of the s-SWCNT/P3HT nanohybrid, indicating the

observed photoresponse is unlikely a thermal effect. In addition, since such a large and fast photoresponse was not observed on s-SWCNTs and P3HT control samples, this result demonstrates that a highly efficient exciton dissociation facilitated by the type-II heterojunctions formed at the s-SWCNT/P3HT interfaces plays a critical role toward photocurrent harvesting in s-SWCNT/P3HT nanohybrids. Further characterizations also rule out the contribution of the P3HT/substrate interface to the exciton dissociation (see Supporting Information).

It should be noted that the photoresponse of a bolometric IR detector follows the same trend of the temperature coefficient of resistance (TCR) as a function of temperature.[29] This is not surprising since the bolometric photoresponse is linearly proportional to the TCR absolute value, which increases monotonically with decreasing temperature for most semiconductors including s-SWCNT (see Figure 3a). In contrast,
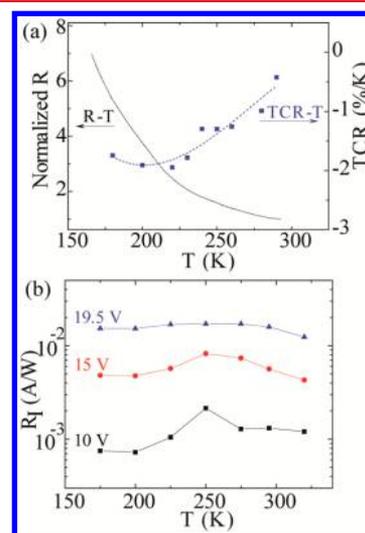

Figure 3. Temperature dependence of s-SWCNT/P3HT nanohybrid's property. (a) $R-T$ (normalized, 5 nA bias) and TCR$-T$ curves, the dashed line is used to show the variation trend. (b) R_I as a function of temperature. The NIR intensity was 2 mW/mm^2.

the photoresponse of the s-SWCNT/P3HT nanohybrid shows a qualitatively different temperature dependence from that of TCR (see Figure 3b). In particular, the TCR absolute value increases by a factor of 4 at about 200 K as compared to its room temperature value. However, no significant changes of NIR photoresponse was observed on the s-SWCNT/P3HT nanohybrids in the temperature range of 175−320 K, and the variation of the current responsivity R_I ($R_I = \Delta I/P$, with ΔI being the photocurrent induced by the charge carriers and can be calculated from the $V-I$ curves as detailed in the Figure S5 of the Supporting Information, P is the power of incident NIR light) is within several tens of percent as shown in Figure 3b, indicating that a thermal response is unlikely a dominant contribution to the observed NIR photoresponse on the s-SWCNT/P3HT nanohybrids.

The R_I and the figure-of-merit D^* are shown as a function of NIR source modulation frequency in Figure 4. $D^* = R_I(A_d)^{1/2}/I_n$, where A_d is the detection area in cm^2 and I_n is the noise current.[29] The R_I decreases monotonically with increasing frequency. At V_{bias} =10 V, R_I decreases from 2.2 mA/W at 10 Hz to 0.94 mA/W at 1 kHz, respectively, as shown in Figure 4a. Note that R_I at 1 kHz only drops by about 40−50% when comparing it with that at 10 Hz, which allows higher D^* to be
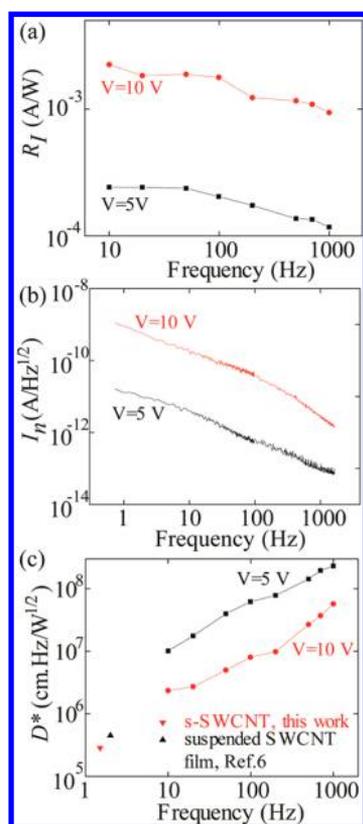
Figure 4. (a) Current responsivity R_I, (b) noise spectra I_n, and (c) detectivity D^* of s-SWCNT/P3HT as a function of modulation frequency at room temperature. NIR light intensity was fixed at 0.35 mW/mm^2 for response measurement.

achieved at a higher frequency due to dominance of $1/f$ noise in the low frequency range. As shown in Figure 4b, the current noise spectra of the s-SWCNT/P3HT nanohybrid decreases monotonically with increasing frequency, which is qualitatively consistent with the trend of standard $1/f$ noise, except for a larger index of $\beta \sim 1.5$ if fitted with $I_n^2 \propto 1/f^{\beta}$. The D^* of s-SWCNT/P3HT shown in Figure 4c varies in an opposite trend and increases monotonically with modulation frequency due to a much more significant decrease of the I_n as compared to R_I with increasing frequency. The maximum D^* obtained at 1 kHz is about 2.3×10^8 cm·Hz$^{1/2}$/W, which to our knowledge is the best that has been observed on CNT IR detectors and is comparable to conventional uncooled IR detectors.[13] It should be noted that the D^* of P3HT/s-SWCNT nanohybrid is at least more than 2 orders of magnitude larger than the maximum D^* of s-SWCNT control sample (this work) and suspended SWCNT film (ref 6) obtained at much lower modulation frequency (due to the limitation of their slow photoresponse), which are also included in Figure 4c as solid dots. The demonstrated high D^* in the s-SWCNT/P3HT nanohybrids confirms the type-II heterojucntion at the s-SWCNT/P3HT interface provides a highly efficient exciton dissociation mechanism, enabling the harvesting of extraordinary photocurrent in high performance CNT NIR photodetectors.

We have successfully demonstrated a significantly improved detectivity D^* up to 2.3×10^8 cm·Hz$^{1/2}$/W in s-SWCNT/P3HT nanohybrid, which shows a great potential of s-SWCNT/P3HT as uncooled IR detectors. The s-SWCNT/P3HT type-II heterojunction interface enables highly efficient

exciton dissociation and extraordinary photocurrent harvesting. The observed D^* of s-SWCNTs/P3HT is more than 2 orders of magnitude higher than that of the pure SWCNT films in both s-SWCNT and as-made forms. A small response time of 1 ms has been confirmed which makes the detector feasible for high-frequency detection of up to 1 kHz while maintaining a high D^* on the order of 10^8 cm·Hz/W$^{1/2}$.

■ ASSOCIATED CONTENT

ⓢ Supporting Information
TEM of s-SWCNT/P3HT nanohybrid, pure s-SWCNT control sample, internal quantum efficiency of s-SWCNT/P3HT nanohybrid, differential conductance of pure s-SWCNT control sample, pure P3HT sample, and $V−I$ curves at different temperatures. This material is available free of charge via the Internet at http://pubs.acs.org.

■ AUTHOR INFORMATION

Corresponding Author
*E-mail: rtlu@ku.edu; jwu@ku.edu.

Notes
The authors declare no competing financial interest.

■ ACKNOWLEDGMENTS

■ REFERENCES

(1) Fujiwara, A.; Matsuoka, Y.; Suematsu, H.; Ogawa, N.; Miyano, K.; Kataura, H.; Maniwa, Y.; Suzuki, S.; Achiba, Y. *Jpn. J. Appl. Phys. Lett.* **2001**, *40* (11B), L1229−L1231.
(2) Xu, J. M. *Infrared Phys. Technol.* **2001**, *42*, 485−491.
(3) Levitsky, I. A.; Euler, W. B. *Appl. Phys. Lett.* **2003**, *83* (9), 1857−1859.
(4) Freitag, M.; Martin, Y.; Misewich, J. A.; Martel, R.; Avouris, P. H. *Nano Lett.* **2003**, *3* (8), 1067−1071.
(5) Itkis, M. E.; Borondics, F.; Yu, A. P.; Haddon, R. C. *Science* **2006**, *312* (5772), 413−416.
(6) Lu, R. T.; Li, Z. Z.; Xu, G. W.; Wu, J. Z. *Appl. Phys. Lett.* **2009**, *94* (16), 163110.
(7) Lai, K. W. C.; Xi, N.; Fung, C. K. M.; Chen, H. Optical response time for carbon nanotube based infrared detectors. In *9th IEEE Conference on Nanotechnology*, Genoa, Italy, 2009.
(8) Lu, R. T.; Shi, J. J.; Baca, J.; Wu, J. Z. *J. Appl. Phys.* **2010**, *108*, 084305.
(9) Wang, F.; Dukovic, G.; Brus, L. E.; Heinz, T. F. *Science* **2005**, *308* (5723), 838−841.
(10) Matsuoka, Y.; Fujiwara, A.; Ogawa, N.; Miyano, K.; Kataura, H.; Maniwa, Y.; Suzuki, S.; Achiba, Y. *Sci. Technol. Adv. Mater.* **2003**, *4*, 47−50.
(11) Mohite, A.; Chakraborty, S.; Gopinath, P.; Sumanasekera, G. U.; Alphenaar, B. W. *Appl. Phys. Lett.* **2005**, *86* (6), 061114.
(12) St-Antoine, B. C.; Menard, D.; Martel, R. *Nano Lett.* **2011**, *11* (2), 609−613.
(13) Chen, C. H.; Yi, X. J.; Zhao, X. R.; Xiong, B. F. *Sens. Actuators, A* **2001**, *90* (3), 212−214.
(14) Bindl, D. J.; Safron, N. S.; Arnold, M. S. *ACS Nano* **2010**, *4* (10), 5657−5664.

(15) Holt, J. M.; Ferguson, A. J.; Kopidakis, N.; Larsen, B. A.; Bult, J.; Rumbles, G.; Blackburn, J. L. *Nano Lett.* **2010**, *10* (11), 4627−4633.

(16) Capaz, R. B.; Spataru, C. D.; Ismail-Beigi, S.; Louie, S. G. *Phys. Rev. B* **2006**, *74* (12), 121401.

(17) Pradhan, B.; Setyowati, K.; Liu, H. Y.; Waldeck, D. H.; Chen, J. *Nano Lett.* **2008**, *8* (4), 1142−1146.

(18) Pradhan, B.; Kohlmeyer, R. R.; Setyowati, K.; Owen, H. A.; Chen, J. *Carbon* **2009**, *47* (7), 1686−1692.

(19) Vera-Reveles, G.; Simmons, T. J.; Bravo-Sanchez, M.; Vidal, M. A.; Navarro-Contreras, H.; Gonzalez, F. J. *ACS Appl. Mater. Interfaces* **2011**, *3* (8), 3200−3204.

(20) Aliev, A. E. *Infrared Phys. Technol.* **2008**, *51* (6), 541−545.

(21) Kazaoui, S.; Minami, N.; Nalini, B.; Kim, Y.; Hara, K. *J. Appl. Phys.* **2005**, *98* (8), 084314.

(22) Kanai, Y.; Grossman, J. C. *Nano Lett.* **2008**, *8* (3), 908−912.

(23) Ren, S. Q.; Bernardi, M.; Lunt, R. R.; Bulovic, V.; Grossman, J. C.; Gradecak, S. *Nano Lett.* **2011**, *11* (12), 5316−5321.

(24) Stranks, S. D.; Weisspfennig, C.; Parkinson, P.; Johnston, M. B.; Herz, L. M.; Nicholas, R. J. *Nano Lett.* **2011**, *11* (1), 66−72.

(25) Zhou, X. J.; Park, J. Y.; Huang, S. M.; Liu, J.; McEuen, P. L. *Phys. Rev. Lett.* **2005**, *95* (14), 146805.

(26) Li, G.; Shrotriya, V.; Yao, Y.; Yang, Y. *J. Appl. Phys.* **2005**, *98*, 4.

(27) Kataura, H.; Kumazawa, Y.; Maniwa, Y.; Umezu, I.; Suzuki, S.; Ohtsuka, Y.; Achiba, Y. *Synth. Met.* **1999**, *103* (1−3), 2555−2558.

(28) Brown, P. J.; Thomas, D. S.; Kohler, A.; Wilson, J. S.; Kim, J. S.; Ramsdale, C. M.; Sirringhaus, H.; Friend, R. H. *Phys. Rev. B* **2003**, *67* (6), 064203.

(29) Dereniak, E. L.; Boreman, G. D. *Infrared Detectors and Systems*; John Wiley & Sons: New York, 1996.